Article

Optical Nanoparticle Sorting Elucidates Synthesis of Plasmonic Nanotriangles

María Ana Huergo, Christoph Matthias Maier, Marcos Federico Castez, Carolina Vericat, Roberto C. Salvarezza, Alexander S. Urban, and Jochen Feldmann

ACS Nano, **Just Accepted Manuscript** • DOI: 10.1021/acsnano.5b08095 • Publication Date (Web): 24 Feb 2016

Optical Nanoparticle Sorting Elucidates Synthesis of Plasmonic Nanotriangles

María Ana Huergo[1,2,3,,‡], Christoph Matthias Maier[2,3,‡], Marcos Federico Castez[1], Carolina Vericat[1], Roberto C. Salvarezza[1], Alexander S. Urban[2,3,*], Jochen Feldmann[2,3]*

1 Instituto de Investigaciones Fisicoquímicas Teóricas y Aplicadas (INIFTA), Universidad Nacional de La Plata – CONICET, Sucursal 4 Casilla de Correo 16, 1900 La Plata, Argentina

2 Chair for Photonics and Optoelectronics, Department of Physics and Center for Nanoscience (CeNS), Ludwig-Maximilians-Universität München, Amalienstraße 54, 80799 Munich, Germany

3 Nanosystems Initiative Munich (NIM), Schellingstraße 4, 80799 Munich, Germany

ABSTRACT

We investigate the optical and morphological properties of gold nanoparticles grown by reducing a gold salt with Na_2S. Lasers are tuned to the observed plasmon resonances, and the optical forces exerted on the nanoparticles are used to selectively print individual nanoparticles onto a substrate. This enables us to combine dark-field spectroscopy and scanning electron microscopy to compare the optical properties of single nanoparticles with their morphology. By arresting the synthesis at different times, we are able to investigate which type of nanoparticle is responsible for the respective resonances. We find that thin Au nanotriangles are the source of the observed NIR resonance. The initial lateral growth of these triangles causes the plasmon resonance to

redshift into the NIR, whereas a subsequent thickening of the triangles and a concomitant truncation lead to a blueshift of the resonance. Furthermore we find that the nanotriangles produced have extremely narrow linewidths (187±23 meV), show nearly isotropic scattering and are stable for long periods of time. This shows their vast potential for applications such as *in-vivo* imaging and bio-(chemical) sensing. The method used here is generally applicable to other syntheses, and shows how complex nanostructures can be built up on substrates by selectively printing NPs of varying plasmonic resonances.

KEYWORDS

Optical printing, gold nanoparticles, cancer therapy, nanoshells, plasmon, nanoparticle sorting

TEXT

Noble metal NPs possess remarkable properties that have led to applications in fields ranging from solar energy harvesting[1-2] and photodetection[3-6] to bio-(chemical) sensing,[7] nanomedicine[8] and cancer therapy.[9-10] One of the main advantages these astounding particles have is the collective oscillation of their conduction band electrons, generally known as ~~a~~ localized surface plasmon (LSP). This leads to an enhanced optical cross section whose resonance position can be tuned by modifying not only the material, but also the size and shape of the NP. Especially interesting for biomedical applications are NPs whose resonance is shifted to the near infrared (NIR) window, a region of minimum absorption in biological tissues between 750 and 900 nm.[11] Nanoshells, comprising a thin metallic film surrounding a dielectric core have proven especially good for this, as the resonance position can be tuned by controlling the ratio of the core to shell radius.[12] One of the proposed synthesis methods of nanoshells consists in the reduction of an Au

salt, $HAuCl_4$, by Na_2S (Figure 1a).[13] It was said that this leads to spherical nanoshells, less than 40 nm in size, with resonances in the NIR window, a strong sensitivity to the surrounding medium and an extremely narrow line width.[14-15] The actual existence of these NPs, however, is a matter of dispute, as some researchers argue that the observed features are either caused by non-spherical Au NPs[16-17] or NP-aggregates.[18-19] Settling this dispute is no easy feat and requires a combination of strategies. Firstly, the synthesis needs to be carried out in a manner that one can investigate the NPs present at any given time during the procedure, as their optical properties change during their growth process. Next, the NPs at each time step need to be separated and their optical properties correlated to their morphology. In case there are many types of particles in the dispersions then one needs a large amount of statistics to be able to draw significant conclusions. Optical forces present an extremely beneficial method for the separation of the individual NPs. Using the strong scattering force acting on plasmonic NPs at resonance it has been possible to print such particles at specific locations onto hard substrates,[20-22] onto phospholipid membranes[23-25] or even to inject them into cells.[24, 26] This effect, termed optical printing, uses a laser tuned to the resonance maximum of the plasmonic NP and consequently the strong axial optical force to propel the NPs along the Poynting vector. Only nanoparticles with particle plasmons in resonance with the laser wavelength experience a force strong enough to propel them towards the surface where they are then affixed. Once a nanoparticle is printed onto the substrate, the printed nanoparticle then interacts with the laser beam, preventing subsequent printing of additional nanoparticles.[22, 27] Additionally, it has been shown that in a dispersion comprising two kinds of metallic NPs, each kind could be propelled in a different direction based on their localized surface plasmon resonance (LSPR), a first step towards NP sorting.[28]

In this manuscript we develop a strategy to settle the aforementioned dispute. The synthesis of the NPs is carried out and arrested at specified times by addition of Na_2S. The NPs are then separated and fixed at specific locations on a substrate through an all-optical approach. By employing multiple lasers we can selectively print NPs whose LSPRs overlap with the laser wavelength. We can then combine dark field Rayleigh scattering and scanning electron microscopy (SEM) to compare the optical properties of the printed NPs with their morphology. Through this method we found that the NPs responsible for the strong NIR peak are not nanoshells, but actually thin Au nanotriangles.[16-17] Additionally, we found that unlike in large nanoprisms, their optical scattering is nearly isotropic, likely due to their small size.[29] Moreover, the nanotriangles possess a very narrow line width and also show a strong sensitivity to the refractive index of the surrounding medium. All of these features are prerequisites for sensing applications, for which these nanotriangles are highly adept. Finally, we propose a mechanism to explain the observed dynamics of the UV-Vis spectra of the NP dispersions during synthesis.

RESULTS AND DISCUSSION

Fabrication of the Au NPs was carried out in a two-step reaction according to previously published methods.[13-14] Briefly, 10 mL of a 2 mM $HAuCl_4$ solution were mixed with 12 mL of fresh 1mM Na_2S solution. After two minutes 2 mL of 1 mM Na_2S solution were added, giving a total molar S/Au ratio of 0.65. The reaction was then allowed to evolve for 3 hours and monitored every two minutes by means of UV-Vis spectroscopy (Figure 1b). The initial UV-Vis spectrum showed a strong peak at 527 nm with a shoulder on the short wavelength side and a very weak signal in the NIR region at 820 nm. As the synthesis progressed, the NIR signal rapidly redshifted within approximately 20 minutes while simultaneously gaining in intensity

(Figure 1c). This peak subsequently blueshifted, initially increasing in intensity and then decreasing again until the peak merged with that of the strong peak in the visible region (see Supporting Information Figure S1). The signal in the green spectral region increased in intensity while only slightly redshifting to 533 nm during the synthesis. This signal is characteristic of small, spherical solid Au NPs with diameters in the range of 20-40 nm,[30] while the NIR peak is the source of the dispute mentioned previously and whose origin we wish to clarify with this work.

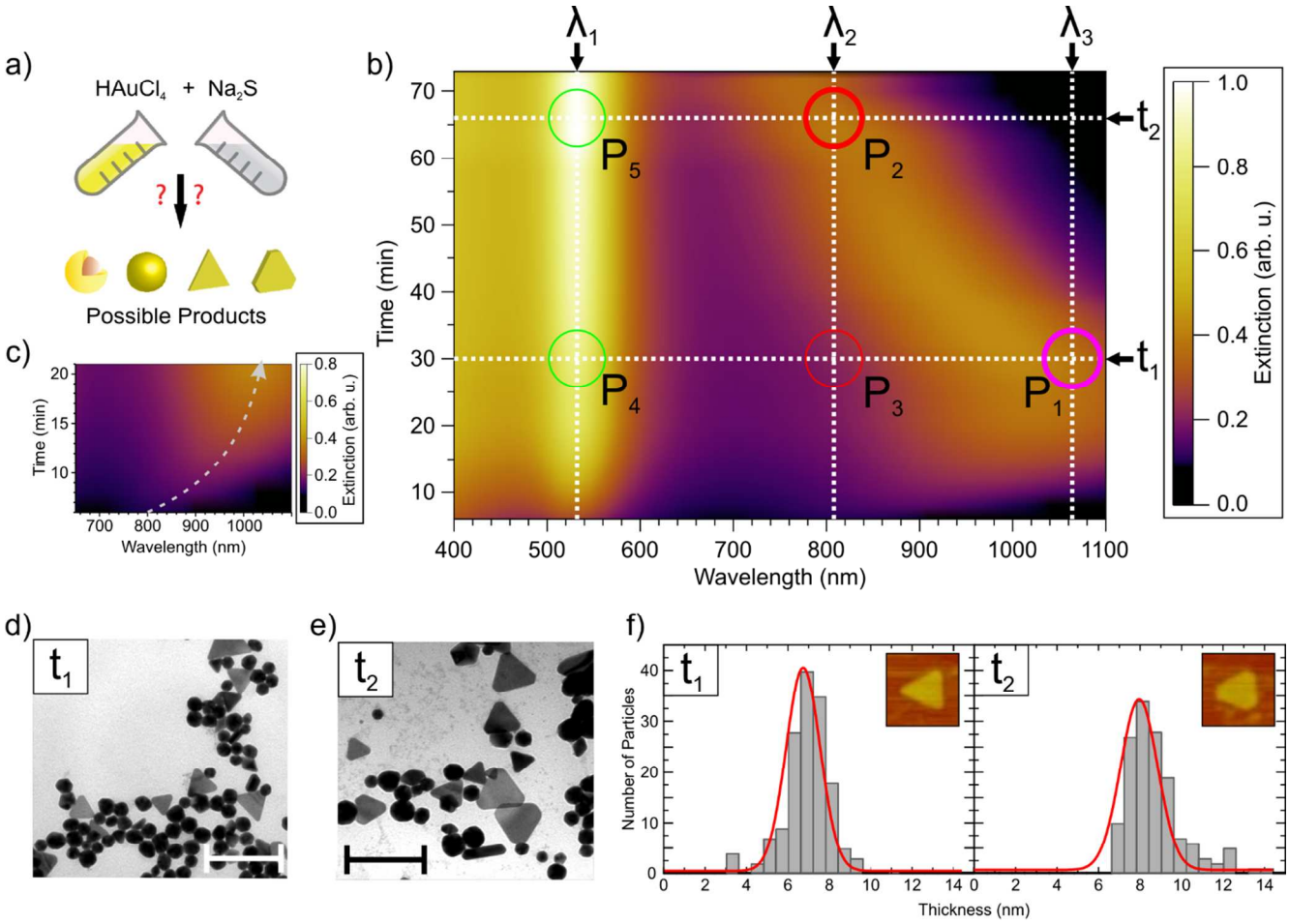

Figure 1. (a) Scheme of the nanoparticle synthesis by reduction of $HAuCl_4$ by Na_2S. (b) Temporal evolution of the extinction spectrum during the synthesis. (c) Magnification showing the initial redshift during the first 20 minutes of the synthesis. TEM images of nanoparticles when arrested at (d) t_1 and (e) t_2. The scale bar is 100 nm. (f) AFM height distribution of nanotriangles from different syntheses, when arrested either at t_1 or t_2. Box size is 150 nm.

In some of the previous studies the initial redshift was purported to stem from the growth of the core of the nanoshells. After 20 minutes the growth of the core terminated and the shell began to grow in thickness. This was said to be the reason for the subsequent observed blueshift of the NIR peak. To investigate these claims we wished to look into the NPs responsible for the NIR resonance at the point of the maximum redshift (time t_1) and then at a later time during the blueshift (time t_2), at an optimal position for biological applications, and at which these NPs have been traditionally analyzed.[13-19] To this end we repeated the synthesis several times, letting it progress until the NIR peak position reached the desired wavelength. The synthesis was then arrested by adding an additional volume of 1 mM Na_2S solution, also leading to high long-term stability of the suspensions (cf. Figure S2).[31] In each synthesis there were slight variations in the UV-Vis spectra, such as the maximum redshift or the speed of evolution; however the general trends were always the same. As a first step we looked at the morphology of the ensemble by means of transmission electron microscopy (TEM) on the two aforementioned dispersions. TEM images of both samples showed large areas covered with tiny (~ 5 nm) NPs (see Figure S3), which we thereupon removed *via* selective centrifugation. In the purified samples we found that the overwhelming majority of remaining NPs (75%) were spherical and between 15 and 40 nm in size (Figure 1d, e). The remaining 25 % of NPs turned out to be equilateral triangles. In the sample stopped at t_1 the majority of these NPs showed were sharp-tipped with side lengths ranging from 60 to 100 nm (Figure 1d). The low contrast of the triangles indicates that they were much thinner than the spheres. This was confirmed by atomic force microscopy (AFM) measurements, which found these triangles to be 6.8 ± 0.7 nm thick (cf. Figure1f and S 4). Additionally, the AFM measurements confirmed that the round NPs were actually spherical in nature. In contrast to the t_1 sample the sample arrested at t_2 was found to contain predominantly

triangles with strongly truncated or rounded corners (Figure 1e). While also having low contrast these triangles were found to be 8.8 ± 1.0 nm thick, which was slightly thicker than those observed in the t_1 sample (see Figure 1f and Figure S4). A small amount of nanorods and more complex looking NPs were also found in both samples. With so many NPs present in each of the samples it was impossible to distinguish which of these were responsible for which features observed in the extinction spectra without investigating them individually. Additionally, the existence of the nanoshells could neither be confirmed nor refuted by these methods.

Therefore we wanted to determine in which way the individual NPs contributed to the UV-Vis spectra and additionally see if nanoshells were present. Our approach consisted of optically sorting the NPs depending on their LSPR, printing them individually on substrates and then comparing their morphology *via* SEM and their optical properties through dark field Rayleigh scattering. To this end we coupled three lasers into an optical dark field microscope whose wavelengths $\lambda_1 = 532\ \text{nm},\ \lambda_2 = 808\ \text{nm},\ \lambda_3 = 1064\ \text{nm}$ overlapped with the previously mentioned UV-Vis peaks (Figure 1b). A diluted drop of each of the dispersions was placed on a glass coverslip and imaged with a water immersion objective. The lasers were focused by the same objective onto the substrates, and printing monitored in the dark field microscope. Once a nanoparticle was printed, the substrate was shifted laterally by several microns. In this manner we were able to print rows of nanoparticles, which could then easily be found in the dark-field and electron microscopes (see Figures S5, 6). When using the 1064 nm laser, the printing could not be observed as easily in the dark field microscope. So, instead of waiting for a printing event, we continuously moved the substrate, in order to avoid long time exposure of printed nanoparticles. The end result however was very similar as for the other two cases.

We wanted to concentrate on two specific points in the UV-Vis spectra, namely the NIR peaks in the t_1 and t_2 dispersions, marked as P_1 and P_2 in Figure 1b. At P_1 NPs were printed rapidly within a matter of seconds using the 1064 nm laser, and all turned out to be sharp-tipped triangles with a large variation in side lengths centered on 70 nm, as confirmed through SEM (Figure 2a).

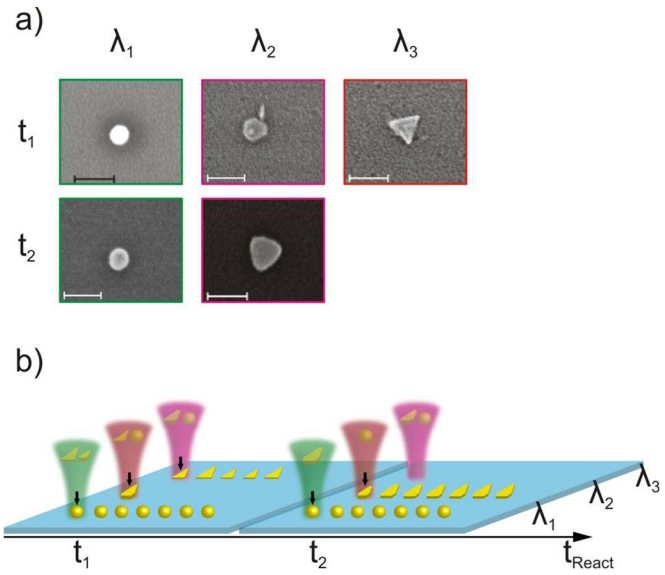

Figure 2. (a) Nanoparticles printed from samples arrested at t_1 and t_2 using laser with the wavelengths λ_1, λ_2 and λ_3 respectively. The scalebars are 100 nm. (b) Scheme of the selective printing process.

Likewise, at P_2 single NPs were printed easily employing the 808 nm laser. These turned out to also be triangles albeit with truncated or rounded edges (Figure 2a). Since there was also a weak signal present at P_3 we also investigated the NPs responsible for this resonance. Printing events only occurred after several minutes, and the printed NPs turned out to be truncated or rounded triangles, like at P_2. This indicates that there are hardly any NPs present in the solution with a plasmon resonance resonant with the laser. No round particles were printed at any of these points. However, when investigating P_4 and P_5 with the 532 nm laser, we were able to rapidly print single spherical NPs, approximately 40 nm in diameter. This method proved to be highly specific as each laser printed NPs of only one type of morphology (Figure 2b, Figures S5, S6). In none of the cases were the printed structures shown to be aggregates of NPs.

In order to check whether the laser affects the nanoparticles during the printing process, we calculated the maximum temperatures of the gold particles by means of the finite element method (FEM, Comsol Multiphysics). With the laser powers used, the maximum temperature increase in the truncated triangles is only around 65 °C. For the sharp-tipped nanotriangles the temperature increase amounts to 245 °C (Figure S7). However this is significantly below the melting temperature of bulk gold and also below that of gold nanoparticles.[32-33] Additionally, in heating experiments of gold nanorods, it was seen that while for thermal heating nanorods transformed completely to spheres at 250 °C within an hour, for laser-induced heating no changes were observed for heating temperatures of up to 700 °C. Since our experiment more resembles the laser-induced heating, as the nanoparticles only experience these temperatures for a very short time due to the constant motion of the substrate, reshaping of the NPs should be negligible.[34-35]

For a full investigation of the individual NPs, their respective morphology needed to be compared to their optical properties. To this end we acquired Rayleigh scattering spectra of optically printed single NPs. All of the spherical NPs showed a strong LSPR around 530 nm, with a width of approximately 400 meV comparable to that of the observed peak in the ensemble UV-Vis measurements (Figure 3a).

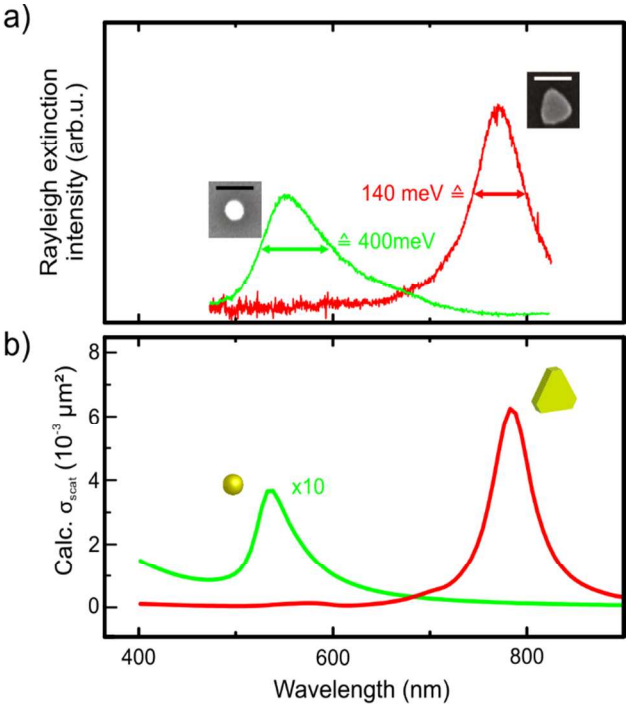

Figure 3. (a) Single particle scattering spectra of printed nanoparticles using the laser wavelengths λ_2 and λ_3. Note the considerably decreased linewidth of the triangular nanoparticle indicating that the huge linewidth of the ensemble is due to inhomogeneous broadening. Scalebars are 100 nm. (b) Scattering cross sections calculated via FDTD of the printed nanoparticles matching the expected peak positions. Simulation parameters were radius = 20 nm for the sphere and side length = 80 nm, clip = 10 nm and thickness = 9 nm for the clipped triangle.

In contrast to this, the truncated nanotriangles all had resonances located between 750 and 800 nm, which were significantly narrower, on the order of only 187 ± 23 meV. This corresponds well to the values reported previously on the purported Au_2S/Au nanoshells[15] and suggests that the broad NIR peak in the UV-Vis spectra was caused by a large inhomogeneous broadening of the nanotriangles in the ensemble. Polarization-dependent measurements showed that the scattering from the nanotriangles was nearly isotropic, a feature generally ascribed to spherical NPs (cf. Figure S8). The narrow linewidth measured should allow for extremely sensitive bio-(chemical) sensing applications, as slight shifts of the refractive index of the medium surrounding the NPs will lead to a large shift of the plasmon resonance (see Figure S9). Based on previous studies and using the values obtained from this analysis we carried out finite difference time domain (FDTD) simulations on the observed NP shapes.[36-42] Using the images obtained from SEM, we are able to reproduce the spectra of the triangles and spheres (Figure 3b).

To corroborate that the nanotriangles alone can reproduce the recorded UV-Vis spectra and explain the red- and subsequent blueshift of the NIR peak during synthesis we carried out a series of simulations and calculations. Statistics of triangle sizes acquired from TEM analysis showed that the side length of the nanotriangles grew during the redshift, reaching a maximum at the time t_1 (Figure 4a). Additionally, the spread in side lengths became considerably broader with

time. Simulated LSPR of sharp-tipped nanotriangles smaller than 50 nm is very weak and located between 650 and 750 nm (Figure 4b). This LSPR redshifts and greatly increases in intensity as the nanotriangles grow, reaching 1000 nm for triangles with 100 nm side length (cf. Figures S10, S11). For truncated triangles, the LSPR blueshifts as the degree of truncation increases, as depicted for triangles of nominal side length 80 nm (Figure 4c). An increasing thickness of both types of nanotriangles, which was measured with an AFM, also leads to a blueshift of the LSPR peak (cf. Figures S12, S13). FDTD simulations of the spheres showed an LSPR around 530 nm, confirming that they are solid Au spheres.[14-15, 43] Combining these findings together we can fully explain the observed UV-VIS spectra (Figure 4d). To achieve this we estimated the distribution of triangle sizes obtained from the TEM, AFM and SEM measurements. We used this to weight the single particle cross sections, taking into account that the ratio of spheres to triangles was approximately 3:1. We compared the resulting individual spectra with the ensemble extinction spectrum obtained from the UV-Vis spectra at t_1 (Figure 4d). The heights of the individual cross sections are normalized with respect to the cross sections of the spheres. The intensity of the individual contributions from the nanotriangles nicely follows the NIR peak, and the intensity ratio of the signal from the spheres to that of the triangles also agrees with the experimental findings, validating the approach we have taken. This shows that the existence of solid Au nanotriangles can fully explain all of the observations made *via* UV-Vis spectroscopy.

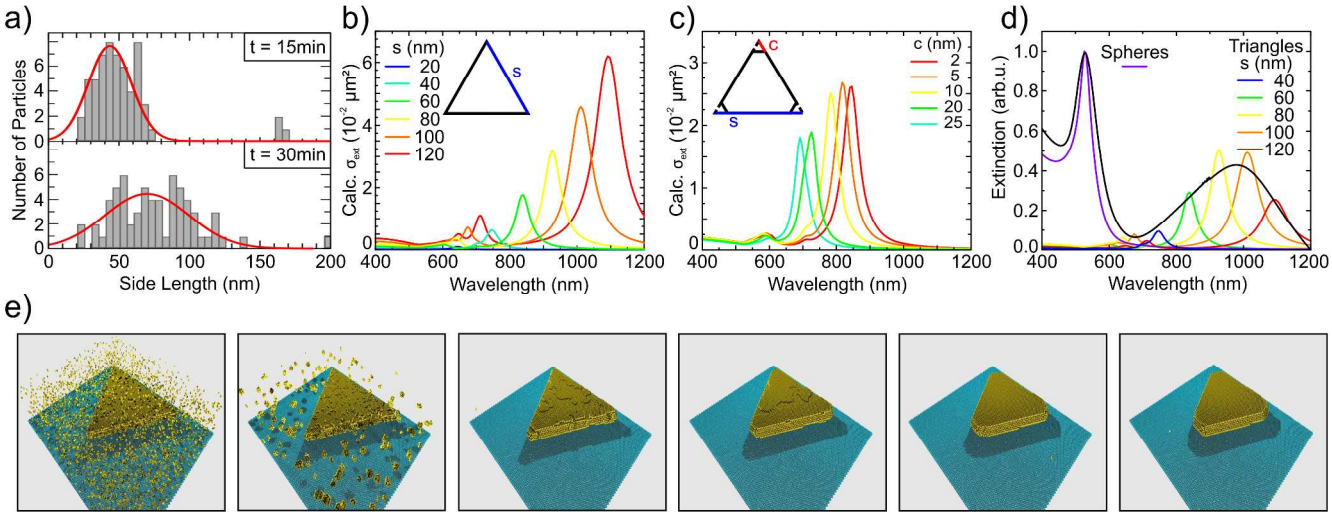

Figure 4. (a) Side lengths of nanotriangles found before (above) and at (below) the maximum red shift. (b) FDTD calculations of extinction cross sections for sharp triangles of thickness, d = 7 nm, with varying side length, s. (c) Calculated extinction cross sections of clipped triangles with d = 9 nm, s = 80 nm for different clip length, c. (d) Weighted spectrum of simulated nanoparticles (colored) in comparison to the measured ensemble spectrum (black). The size distribution of sharp triangles was taken from Fig. 4a, t = 30min and the intensities from Fig. 4b were weighted correspondingly. The spectrum of spherical 40nm gold nanoparticles was multiplied by three due to the ratio of spheres to triangles of roughly 3:1. The measured ensemble spectrum was normalized to the peak of the simulated spherical nanoparticles. (e) Monte Carlo simulation of the evolution of a sharp thin nanotriangle to a truncated thicker one for zero, 100, 1000, 2500, 5000 and 10000 Monte Carlo steps.

While the synthesis of different nanotriangles has been long investigated,[44-46] studies on the structural changes of the NPs as their synthesis progresses are lacking. It is known that particle shape results from two competitive phenomena: growth far from equilibrium (fast Au atom aggregation) that results in tip formation, and thermodynamics that tends to smooth out these instabilities by slow surface diffusion processes.[47] We believe that the truncation of originally sharp-tipped nanotriangles is the result of both intraparticle Au atom diffusion and the Au incorporation from non-reduced Au species (from excess reactant) and the small NPs present in the solution through an Ostwald ripening process. Thus, depending on the reaction time, one of these two phenomena prevails, explaining the initial redshift (kinetics) and the final blueshift (thermodynamics) experimentally observed.

We performed Monte Carlo (MC) simulations to mimic the structural transformations that sharp nanotriangles may experience in the presence of an Au atom source (for details see: Supporting Information). For the initial condition we started with a triangular Au NP with sharp edges surrounded by a random dispersion of Au atoms occupying 1% of the available sites (Figure 4e). Once the simulation commenced these Au atoms rapidly agglomerated, forming small clusters. These then condensed on the nanotriangles through an Ostwald ripening process. Mass transport by surface diffusion subsequently led to Au atoms wandering from the tips and sides to the large top surface, increasing the thickness and rounding the sharp tips. Considering

all of the obtained results we have devised a model to explain the observed dynamics of the UV-Vis spectra during the synthesis. Initially the synthesis produces two main types of NPs, solid Au spheres and thin triangles. As the synthesis progresses the spheres become slightly larger in size, while the triangles became significantly larger. Once the latter reach side lengths of ≈50 nm, their extinction cross sections become large enough to be discernible from the spheres in the UV-Vis spectra. As the synthesis progresses triangles become larger, but at different rates, so the spread in sizes becomes greater, leading in turn to a larger inhomogeneous broadening. The triangles then become truncated and thicker, producing the observed blue-shift and explaining the slight decrease in inhomogeneous broadening, as the LSPR positions of thicker nanotriangles are not quite as dependent on side length as the thinner ones are. This model also agrees with experiments showing the formation and growth of silver nanotriangles.[48]

CONCLUSIONS

In summary we have used optical printing and single particle spectroscopy to investigate the synthesis of Au NPs by the reduction of $HAuCl_4$ with Na_2S. UV-Vis spectra showed a strong peak in the NIR that first redshifted in time and subsequently blueshifted. By stopping the synthesis at different times and employing lasers tuned to the UV-Vis peaks of these dispersions, we were able to determine which NPs were responsible for the observed resonances. Single NPs whose resonance overlapped with the laser wavelength were printed onto substrates. Rayleigh scattering spectra of these single NPs were acquired and compared with SEM images. We found that, contrary to previous reports, the NPs responsible for the NIR peak are neither nanoshells comprising an Au shell around an Au_2S core nor Au NP aggregates, but actually thin, solid Au nanotriangles. By arresting the reaction at different times we studied the structural evolution of

the nanotriangles and the corresponding effect on their optical properties. The initial redshift is caused by the lateral growth of these triangles. The subsequent blueshift is a result of the simultaneous increasing thickness and degree of rounding or truncation of the nanotriangle tips as was confirmed by MC simulations. FDTD calculations confirmed measurements showing that the linewidth of the nanotriangles is extremely narrow, less than 190 meV, and that small variations in size, thickness and truncation lead to the large inhomogeneous linewidth of the ensembles. These optical properties along with the long-term stability of the nanotriangles show the great potential of the Au nanotriangles in various applications, such as *in-vivo* imaging and bio-(chemical) sensing. Optical forces have proven an important tool not only for surface patterning of substrates but also as a means to investigate chemical reactions and optical properties of NPs. Additionally, the use of multiple laser wavelengths tuned to individual plasmon resonances will permit surface structuring simultaneously with a multitude of different pre-formed plasmonic NPs, leading to further possible applications in chemical and bio-sensing, fluorescence enhancement and photodetection.

METHODS

Gold Nanoparticle Synthesis

Gold nanoparticles were synthesized at room temperature in a two-step reaction by reduction of $HAuCl_4$ (G4022 Sigma Aldrich) with Na_2S (407410 Sigma Aldrich), as reported elsewhere.[14] In a typical procedure, 10 mL of a 2 mM $HAuCl_4$ solution were mixed with 12 mL of fresh 1mM Na_2S solution (pH = 6). After two minutes 2 mL 1 mM Na_2S solution were added, giving a total molar S/Au ratio of 0.65. The reaction was then allowed to evolve for different times, between 5 minutes and 3 hours, and then 14 mL of 1 mM Na_2S solution was added to arrest its evolution.

Nanoparticle printing

For the particle printing experiments, cw-lasers of wavelengths 532nm (Coherent Verdi V10, Coherent, USA), 1064nm (Cobolt Rumba 05-10, Cobolt, Sweden) and a Ti:Sapphire Oscillator (Spectra-Physics Tsunami, Spectra-Physics, USA) pumped by a 532nm Spectra-Physics Millenia V (Spectra-Physics, USA) operated in cw mode at 808nm were sequentially coupled into an upright Zeiss Axiotech 100 (Zeiss, Germany) microscope. The laser beams were focused by a Zeiss Achroplan 100x/1.0W water dipping objective (Zeiss, Germany) which was dipped directly into the diluted nanoparticle dispersion of interest. In order to correct for the chromatic aberration of the objective appearing in the NIR, the 1064nm laser was prefocused by a lens with f=1000mm placing the laser focus in the image plane. Nanoparticles were made visible by applying dark field conditions using a dark field condenser placed in the light path.[49]

For printing at 808 and 1064nm a laser power around 15mW on the sample was used. The power was set so that the average time between two printing events was on the scale of 5s. At 532nm a lower laser power of around 5mW on the sample was enough due to the significantly higher concentration of resonant spherical particles. The particle dispersion was diluted 1:100 with MiliQ water before printing. More water was added during the experiment to compensate for evaporation keeping the particle concentration constant. The laser spot sizes were around 1μm. After each printing event, the piezo stage was moved by several microns to avoid printing of multiple particles in close vicinity.

The area where the nanoparticles were printed was marked by a scratch to allow their later relocation for single particle spectroscopy and SEM. After the optical printing was performed samples were rinsed carefully with MiliQ water to remove the nanoparticle dispersion avoiding further random deposition.

Single particle spectroscopy

Single particle spectra were acquired using an upright Zeiss AxioLab.A1 microscope in dark field condition attached to a Princeton Instruments SP2300 monochromator (Princeton Instruments, USA) together with an LN-cooled CCD (Acton Spec-10, Princeton Instruments, USA).

Scanning electron microscopy (SEM)

The individual printed nanoparticles were imaged using a Zeiss Ultra 55 Plus SEM (Zeiss, Germany). In order to avoid electrical charging of the substrate a thin (~1nm) layer of a gold-palladium alloy was sputtered on top of the substrate with a Leica Sputter Coater EM SCD005 (Leica Microsystems, Germany) making the substrate's surface conductive.

Transmission Electron Microscopy (TEM)

TEM samples were prepared by deposing 7 μL of arrested nanoparticle dispersion onto a carbon coated copper TEM grid (Ted Pella, USA) which was left to dry in the dark and subsequently measured with a JEOL JEM-1011 TEM (JEOL, Japan)

UV-Vis Spectroscopy

Extinction spectra of the nanoparticle dispersion at different stages of the synthesis were taken with an Agilent Cary 60 Spectrophotometer.

Atomic Force Microscopy (AFM)

AFM experiments were performed in air in tapping mode with a multimode microscope operated by a Nanoscope V control unit, both from Veeco Instruments (Bruker Corporation, USA). Silicon tips from NanoWorld (Switzerland) were used in all measurements at f_o = 285 kHz; k = 42 N/m. Samples were prepared by drop-casting the nanoparticle dispersions on freshly cleaved HOPG substrates (Ted Pella Inc., USA).

Simulations of effective extinction and scattering cross sections:

Effective cross sections were calculated using the software Lumerical FDTD Solutions (Lumerical, Vancouver, Canada). The simulation environment measured 2000 x 2000 x 2000 nm^3 applying 24 perfectly matched layers with a reflection coefficient of 0.0001. The gold nanoparticles were modeled by interpolating the dielectric functions of gold and water from the measured data of Johnson and Christy[50] and Palik[51] respectively and placed in the middle of simulation volume filled up with water. The particles were surrounded by a mesh with a cell size of 0.05nm. The linearly polarized electromagnetic plane-wave was injected in positive z-direction, resembling the dark field illumination used in the experiments. The simulation time was chosen to be 1000 fs after which convergence was attained.

Simulation of particle temperatures

The temperatures the nanoparticles have during the printing process were calculated by using finite elements method (Comsol Multiphysics 5.2, COMSOL, Sweden). Therefore we determined the laser power density by first imaging the laser spot and then fitting a 2D Gaussian function. We then integrated this Gaussian over the previously calculated absorption cross-section of the particular particles at the printing wavelength. Knowing the total laser power this gives us the absorbed laser power density which is converted to heat.

In COMSOL we modeled the dimensions of the particular sharp and clipped triangles in a water surrounding. Giving the structure the calculated absorbed laser power density leads to the calculated equilibrium temperature.

Monte Carlo Simulations

We have implemented a kinetic Monte Carlo model in which particles are able to perform diffusion events between nearest neighbors in an FCC lattice. Transition probabilities

$P(c_{ini} \rightarrow c_{fin})$ from a given initial configuration c_{ini} into c_{fin} were taken according to the transition state theory, *i.e.*

$$P(c_{ini} \rightarrow c_{fin}) = \nu \exp[-E_{act}(c_{ini} \rightarrow c_{fin})/k_B T$$

where ν is the attempt frequency set equal to 5×10^{12} Hz, $E_{act}(c_{ini} \rightarrow c_{fin})$ is the activation energy for the transition, k_B is the Boltzmann constant, and T is the absolute temperature.

We have chosen a simple model[52-53] for the activation energies, in which a linear dependence of the energy barrier with the first-neighbor coordination number (n) of the diffusing particle at the initial state is assumed: $E_{act} = E_b \cdot n$, where E_b can be interpreted as the bond energy between two nearest neighbor particles (in this work, we have set E_b = 0.1 eV and T=300 K).

ASSOCIATED CONTENT

Supporting Information. The following material is included: Extinction spectra showing: synthesis after 24 hours, long-term stability of samples after synthesis was arrested. Additional TEM, AFM, SEM images depicting nanoparticles found in the samples. Comparison of experimental and calculated polarization-dependent scattering spectra on nanotriangles. Calculated extinction spectra showing the dependence of the spectra on surrounding medium, nanotriangle thickness, degree of truncation, and size. This material is available free of charge *via* the Internet at http://pubs.acs.org.

AUTHOR INFORMATION

Corresponding Authors

* MAH: mahuergo@inifta.unlp.edu.ar;

* ASU: urban@lmu.de.

Author Contributions

The manuscript was written through contributions of all authors. All authors have given approval to the final version of the manuscript. ‡These authors contributed equally.

Funding Sources

This work was supported by the ERC through the Advanced Investigator Grant HYMEM, by ANPCyT (PICT 2010-2554 and 2012-0836) and CONICET (PIP 112-200801-00362 and 112-201201-00093). M.A.H would like to acknowledge the DAAD for sponsoring a postdoctoral fellowship.

ACKNOWLEDGMENT

We thankfully acknowledge P. Kühler for access to his code for FDTD simulations and T. Lohmüller for helpful discussions.

ABBREVIATIONS

LSP, localized surface plasmon; LSPR, localized surface plasmon resonance; NIR, near infrared; SEM, scanning electron microscopy; TEM, transmission electron microscopy; AFM, atomic force microscopy; FDTD, finite difference time domain; MC, Monte Carlo; NP, nanoparticle; Au, gold.

REFERENCES

(1) Catchpole, K. R.; Polman, A. Plasmonic Solar Cells. *Opt. Express.* **2008,** 16, 21793-21800.

(2) Hogan, N. J.; Urban, A. S.; Ayala-Orozco, C.; Pimpinelli, A.; Nordlander, P.; Halas, N. J. Nanoparticles Heat through Light Localization. *Nano Lett.* **2014,** 14, 4640-4645.

(3) Knight, M. W.; Sobhani, H.; Nordlander, P.; Halas, N. J. Photodetection with Active Optical Antennas. *Science.* **2011,** 332, 702-704.

(4) Knight, M. W.; Wang, Y.; Urban, A. S.; Sobhani, A.; Zheng, B. Y.; Nordlander, P.; Halas, N. J. Embedding Plasmonic Nanostructure Diodes Enhances Hot Electron Emission. *Nano Lett.* **2013,** 13, 1687-92.

(5) Bek, A.; Jansen, R.; Ringler, M.; Mayilo, S.; Klar, T. A.; Feldmann, J. Fluorescence Enhancement in Hot Spots of AFM-Designed Gold Nanoparticle Sandwiches. *Nano Lett.* **2008,** 8, 485-490.

(6) Ringler, M.; Schwemer, A.; Wunderlich, M.; Nichtl, A.; Kürzinger, K.; Klar, T. A.; Feldmann, J. Shaping Emission Spectra of Fluorescent Molecules with Single Plasmonic Nanoresonators. *Phys. Rev. Lett.* **2008,** 100, 203002.

(7) Saha, K.; Agasti, S. S.; Kim, C.; Li, X.; Rotello, V. M. Gold Nanoparticles in Chemical and Biological Sensing. *Chem. Rev.* **2012,** 112, 2739-2779.

(8) Boisselier, E.; Astruc, D. Gold Nanoparticles in Nanomedicine: Preparations, Imaging, Diagnostics, Therapies and Toxicity. *Chem. Soc. Rev.* **2009,** 38, 1759-1782.

(9) Urban, C.; Urban, A. S.; Charron, H.; Joshi, A. Externally Modulated Theranostic Nanoparticles. *Transl. Cancer Res.* **2013,** 2, 292-308.

(10) Ayala-Orozco, C.; Urban, C.; Bishnoi, S.; Urban, A.; Charron, H.; Mitchell, T.; Shea, M.; Nanda, S.; Schiff, R.; Halas, N.; Joshi, A. Sub-100nm Gold Nanomatryoshkas Improve Photo-

Thermal Therapy Efficacy in Large and Highly Aggressive Triple Negative Breast Tumors. *J. Controlled Release.* **2014,** 191, 90-97.

(11) Dickerson, E. B.; Dreaden, E. C.; Huang, X.; El-Sayed, I. H.; Chu, H.; Pushpanketh, S.; McDonald, J. F.; El-Sayed, M. A. Gold Nanorod Assisted near-Infrared Plasmonic Photothermal Therapy (Pptt) of Squamous Cell Carcinoma in Mice. *Cancer Lett.* **2008,** 269, 57-66.

(12) Halas, N. The Optical Properties of Nanoshells. *Opt. Photon. News.* **2002,** 13, 26-30.

(13) Zhou, H. S.; Honma, I.; Komiyama, H.; Haus, J. W. Controlled Synthesis and Quantum-Size Effect in Gold-Coated Nanoparticles. *Phys. Rev. B.* **1994,** 50, 12052-12056.

(14) Averitt, R. D.; Sarkar, D.; Halas, N. J. Plasmon Resonance Shifts of Au-Coated Au2s Nanoshells: Insight into Multicomponent Nanoparticle Growth. *Phys. Rev. Lett.* **1997,** 78, 4217-4220.

(15) Raschke, G.; Brogl, S.; Susha, A. S.; Rogach, A. L.; Klar, T. A.; Feldmann, J.; Fieres, B.; Petkov, N.; Bein, T.; Nichtl, A.; Kürzinger, K. Gold Nanoshells Improve Single Nanoparticle Molecular Sensors. *Nano Lett.* **2004,** 4, 1853-1857.

(16) Mikhlin, Y.; Likhatski, M.; Karacharov, A.; Zaikovski, V.; Krylov, A. Formation of Gold and Gold Sulfide Nanoparticles and Mesoscale Intermediate Structures in the Reactions of Aqueous $HAuCl_4$ with Sulfide and Citrate Ions. *Phys. Chem. Chem. Phys.* **2009,** 11, 5445-5454.

(17) Diao, J. J.; Chen, H. Near Infrared Surface Plasmon Resonance of Gold Tabular Nanostructures in the $HAuCl_4$–Na_2S Reaction. *J. Chem. Phys.* **2006,** 124, 116103.

(18) Schwartzberg, A.; Grant, C.; Van Buuren, T.; Zhang, J. Reduction of $HAuCl_4$ by Na_2S Revisited: The Case for Au Nanoparticle Aggregates and against Au_2S/Au Core/Shell Particles. *J. Phys. Chem. C.* **2007,** 111, 8892-8901.

(19) Zhang, J. Z.; Schwartzberg, A. M.; Norman, T.; Grant, C. D.; Liu, J.; Bridges, F.; van Buuren, T. Comment on "Gold Nanoshells Improve Single Nanoparticle Molecular Sensors". *Nano Lett.* **2005,** 5, 809-810.

(20) Nedev, S.; Urban, A. S.; Lutich, A. A.; Feldmann, J. Optical Force Stamping Lithography. *Nano Lett.* **2011,** 11, 5066-5070.

(21) Urban, A. S.; Fedoruk, M.; Nedev, S.; Lutich, A.; Lohmueller, T.; Feldmann, J. Shrink-to-Fit Plasmonic Nanostructures. *Adv. Opt. Mater.* **2013,** 1, 123-127.

(22) Urban, A. S.; Lutich, A. A.; Stefani, F. D.; Feldmann, J. Laser Printing Single Gold Nanoparticles. *Nano Lett.* **2010,** 10, 4794-4798.

(23) Urban, A. S.; Fedoruk, M.; Horton, M. R.; Radler, J.; Stefani, F. D.; Feldmann, J. Controlled Nanometric Phase Transitions of Phospholipid Membranes by Plasmonic Heating of Single Gold Nanoparticles. *Nano Lett.* **2009,** 9, 2903-2908.

(24) Urban, A. S.; Pfeiffer, T.; Fedoruk, M.; Lutich, A. A.; Feldmann, J. Single-Step Injection of Gold Nanoparticles through Phospholipid Membranes. *ACS Nano.* **2011,** 5, 3585-3590.

(25) Ba, H.; Rodríguez-Fernández, J.; Stefani, F. D.; Feldmann, J. Immobilization of Gold Nanoparticles on Living Cell Membranes Upon Controlled Lipid Binding. *Nano Lett.* **2010,** 10, 3006-3012.

(26) Li, M.; Lohmüller, T.; Feldmann, J. Optical Injection of Gold Nanoparticles into Living Cells. *Nano Lett.* **2015,** 15, 770-775.

(27) Gargiulo, J.; Cerrota, S.; Cortés, E.; Violi, I. L.; Stefani, F. D. Connecting Metallic Nanoparticles by Optical Printing. *Nano Lett.* **2016,** 16, 1224-1229.

(28) Ploschner, M.; Čižmár, T.; Mazilu, M.; Di Falco, A.; Dholakia, K. Bidirectional Optical Sorting of Gold Nanoparticles. *Nano Lett.* **2012,** 12, 1923-1927.

(29) Viarbitskaya, S.; Teulle, A.; Marty, R.; Sharma, J.; Girard, C.; Arbouet, A.; Dujardin, E. Tailoring and Imaging the Plasmonic Local Density of States in Crystalline Nanoprisms. *Nat. Mater.* **2013,** 12, 426-432.

(30) Link, S.; El-Sayed, M. A. Size and Temperature Dependence of the Plasmon Absorption of Colloidal Gold Nanoparticles. *J. Phys. Chem. B.* **1999,** 103, 4212-4217.

(31) Zweifel, D. A.; Wei, A. Sulfide-Arrested Growth of Gold Nanorods. *Chem. Mater.* **2005,** 17, 4256-4261.

(32) Castro, T.; Reifenberger, R.; Choi, E.; Andres, R. P. Size-Dependent Melting Temperature of Individual Nanometer-Sized Metallic Clusters. *Phys. Rev. B.* **1990,** 42, 8548-8556.

(33) Schmid, G.; Corain, B. Nanoparticulated Gold: Syntheses, Structures, Electronics, and Reactivities. *Eur. J. Inorg. Chem.* **2003,** 2003, 3081-3098.

(34) Ni, W.; Ba, H.; Lutich, A. A.; Jäckel, F.; Feldmann, J. Enhancing Single-Nanoparticle Surface-Chemistry by Plasmonic Overheating in an Optical Trap. *Nano Lett.* **2012,** 12, 4647-4650.

(35) Petrova, H.; Perez Juste, J.; Pastoriza-Santos, I.; Hartland, G. V.; Liz-Marzan, L. M.; Mulvaney, P. On the Temperature Stability of Gold Nanorods: Comparison between Thermal and Ultrafast Laser-Induced Heating. *Phys. Chem. Chem. Phys.* **2006,** 8, 814-821.

(36) Myroshnychenko, V.; Rodríguez-Fernández, J.; Pastoriza-Santos, I.; Funston, A. M.; Novo, C.; Mulvaney, P.; Liz-Marzán, L. M.; de Abajo, F. J. G. Modelling the Optical Response of Gold Nanoparticles. *Chem. Soc. Rev.* **2008,** 37, 1792-1805.

(37) Shuford, K. L.; Ratner, M. A.; Schatz, G. C. Multipolar Excitation in Triangular Nanoprisms. *J. Chem. Phys.* **2005,** 123, 114713.

(38) Ringe, E.; Langille, M. R.; Sohn, K.; Zhang, J.; Huang, J.; Mirkin, C. A.; Van Duyne, R. P.; Marks, L. D. Plasmon Length: A Universal Parameter to Describe Size Effects in Gold Nanoparticles. *J. Phys. Chem. Lett.* **2012,** 3, 1479-1483.

(39) Kelly, K. L.; Coronado, E.; Zhao, L. L.; Schatz, G. C. The Optical Properties of Metal Nanoparticles: The Influence of Size, Shape, and Dielectric Environment. *J. Phys. Chem. B.* **2003,** 107, 668-677.

(40) Jain, P. K.; Lee, K. S.; El-Sayed, I. H.; El-Sayed, M. A. Calculated Absorption and Scattering Properties of Gold Nanoparticles of Different Size, Shape, and Composition: Applications in Biological Imaging and Biomedicine. *J. Phys. Chem. B.* **2006,** 110, 7238-7248.

(41) Henry, A.-I.; Bingham, J. M.; Ringe, E.; Marks, L. D.; Schatz, G. C.; Van Duyne, R. P. Correlated Structure and Optical Property Studies of Plasmonic Nanoparticles. *J. Phys. Chem. C.* **2011,** 115, 9291-9305.

(42) Mock, J. J.; Barbic, M.; Smith, D. R.; Schultz, D. A.; Schultz, S. Shape Effects in Plasmon Resonance of Individual Colloidal Silver Nanoparticles. *J. Chem. Phys.* **2002,** 116, 6755-6759.

(43) Sönnichsen, C.; Franzl, T.; Wilk, T.; Plessen, G. v.; Feldmann, J. Plasmon Resonances in Large Noble-Metal Clusters. *New J. Phys.* **2002,** 4, 93.

(44) Shankar, S. S.; Bhargava, S.; Sastry, M. Synthesis of Gold Nanospheres and Nanotriangles by the Turkevich Approach. *J. Nanosci. Nanotechno.* **2005,** 5, 1721-1727.

(45) Ah, C. S.; Yun, Y. J.; Park, H. J.; Kim, W.-J.; Ha, D. H.; Yun, W. S. Size-Controlled Synthesis of Machinable Single Crystalline Gold Nanoplates. *Chem. Mater.* **2005,** 17, 5558-5561.

(46) Scarabelli, L.; Coronado-Puchau, M.; Giner-Casares, J. J.; Langer, J.; Liz-Marzán, L. M. Monodisperse Gold Nanotriangles: Size Control, Large-Scale Self-Assembly and Performance in Surface-Enhanced Raman Scattering. *ACS Nano.* **2014,** 8, 5833-5842.

(47) Barabási, A.-L.; Stanley, H. E. *Fractal Concepts in Surface Growth*. Cambridge University Press: Cambridge, GB, 1995.

(48) Jiang, X.; Zeng, Q.; Yu, A. Thiol-Frozen Shape Evolution of Triangular Silver Nanoplates. *Langmuir.* **2007,** 23, 2218-2223.

(49) Sönnichsen, C.; Geier, S.; Hecker, N.; Von Plessen, G.; Feldmann, J.; Ditlbacher, H.; Lamprecht, B.; Krenn, J.; Aussenegg, F.; Chan, V. Z. Spectroscopy of Single Metallic Nanoparticles Using Total Internal Reflection Microscopy. *Appl. Phys. Lett.* **2000,** 77, 2949-2951.

(50) Johnson, P. B.; Christy, R. W. Optical Constants of the Noble Metals. *Phys. Rev. B.* **1972,** 6, 4370.

(51) Querry, M. R.; Wieliczka D. M.; Segelstein, D. J. Water (H_2O) In *Handbook of Optical Constants of Solids*; Palik, E.D., Ed.; Academic Press: Orlando, 1997; pp 1059-1077.

(52) Combe, N.; Jensen, P.; Pimpinelli, A. Changing Shapes in the Nanoworld. *Phys. Rev. Lett.* **2000,** 85, 110.

(53) Iguain, J. L.; Lewis, L. J. Relaxation Kinetics in Two-Dimensional Structures. *Phys. Rev. B.* **2003,** 68, 195407.

TOC GRAPHIC